Alternative Methods for Wet-Dry Cycling of Geosynthetic Clay Liners

Faith Zangl[1] and William J. Likos, M.ASCE[2]

Abstract: Alternative laboratory approaches for cyclic permeation-desiccation experiments on geosynthetic clay liner (GCL) specimens are compared. Permeation cycles for hydraulic conductivity (k) are conducted in flexible-wall permeameters. Subsequent desiccation cycles are conducted using one of three approaches: (1) unconfined desiccation involving drying under controlled relative humidity (RH) with no external stress; (2) axially constrained desiccation involving drying under controlled RH and axial stress simulating one meter of cover soil; and (3) a novel in-permeameter method, where specimens are desiccated without physical disturbance by flushing the permeameter endcaps with controlled-RH gas. Comparison metrics include image analysis of bentonite crack patterns, cycle duration, uniformity of water content, and evolution of k for up to seven wet-dry cycles. All three methods result in similar water content, crack intensity, and hydraulic conductivity response, despite the fact that stress conditions during drying and disturbance to specimens are very different. Observed similarity indicates that internal flaws in the bentonite (e.g., reinforcing fibers), rather than external stress conditions, control desiccation crack initiation and propagation. DOI: 10.1061/(ASCE)GT.1943-5606.0001508. © 2016 American Society of Civil Engineers.

Author keywords: Geosynthetic clay liner (GCL); Desiccation; Bentonite; Hydraulic conductivity; Cracking.

Introduction

Geosynthetic clay liners (GCLs) are composite materials containing a thin layer of bentonite (~5–10 mm) sandwiched between two geotextile layers. The functional component of a GCL is the bentonite layer, which ideally is comprised predominately of sodium (Na^b) montmorillonite clay, meaning that sodium is the predominant species associated with the cation exchange complex. When exposed to water, Na-bentonite (herein Na-B) is capable of a high degree of osmotic interlayer swelling and thus develops very low saturated hydraulic conductivity ($k \sim 1 \times 10^{-11}$ m=s) after hydration (Shan and Daniel 1991; Shackelford et al. 2000; Jo et al. 2001, 2005; Kolstad et al. 2004). This attribute has led to widespread use of GCLs in a variety of waste containment and barrier applications.

Numerous studies have confirmed that osmotic swelling can be inhibited and hydraulic conductivity (k) can be three to four orders of magnitude higher than desired if the bentonite in a GCL is not fully hydrated or if cation exchange has resulted in a predominantly polyvalent cation exchange complex (Egloffstein 2001; Melchior 2002; Benson et al. 2007; Meer and Benson 2007). Laboratory tests and field observation of GCLs exhumed from in-service cover systems have indicated extensive cracking attributable to concurrent desiccation, cation exchange, and cracks that may not fully heal upon rehydration (e.g., James et al. 1997; Egloffstein 2001; Henken-Mellies et al. 2002; Mackey and Olsta 2004; Benson et al. 2007; Meer and Benson 2007; Scalia and Benson 2011).

Several laboratory studies have examined the coupled effects of cation exchange and wet-dry cycling on the swelling and k behavior of GCLs (e.g., Shan and Daniel 1991; Daniel et al. 1993; Boardman and Daniel 1997; Lin and Benson 2000; Sporer and Gartung 2002; Sivakumar Babu et al. 2002; Benson and Meer 2009; Mazzieri 2011). Similar studies of thermal desiccation in composite liner systems have also been explored (e.g., Azad et al. 2011). Experimental techniques to hydrate and subsequently desiccate specimens in such studies have varied widely in terms of confining stress, drying environment (relative humidity, temperature), number of wet-dry cycles, and chemistry of permeant solutions. Many such procedures have required potentially damaging handling of specimens (e.g., disassembly and removal from the permeameter) and in some cases, have resulted in nonrepresentative shrinkage deformations (e.g., extensive curling) if external stress is not applied to the GCL during drying. Such conditions are not representative of field conditions where cover soils apply overburden stress and free shrinkage is restrained. Corresponding impacts to measured k behavior remain largely unknown.

In this study, three alternative approaches for conducting cyclic wet-dry experiments on laboratory GCL specimens are assessed and compared. Conventional Na-B GCLs were permeated in flexible-wall permeameters to determine k according to ASTM D5084 (ASTM 2003) using either deionized water (DW) or a conservative water (CW) solution representing pore fluid chemistry of landfill cover soils. Specimens were desiccated using three approaches: (1) an unconfined desiccation method using a controlled relative humidity (RH) chamber with no external stress applied to the specimen; (2) an axially constrained method using the same controlled RH chamber but under an axial stress simulating ~1 m of cover soil; and (3) an in-permeameter method, where specimens were desiccated without the requirement to remove them from the permeameter by actively flushing the endcaps with controlled-humidity gas. Specimens were then hydrated, permeated to determine steady-state k, and desiccated again for up to as many as seven cycles depending on the method adopted.

[1]Staff Engineer, GEI Consultants Inc., 3159 Voyager Dr., Green Bay, WI 54311. E-mail: fzangl@geiconsultants.com

[2]Professor, Geological Engineering, Univ. of Wisconsin-Madison, Madison, WI 53706 (corresponding author). E-mail: likos@wisc.edu

Note. This manuscript was submitted on April 29, 2015; approved on January 26, 2016; published online on June 23, 2016. Discussion period open until November 23, 2016; separate discussions must be submitted for individual papers. This paper is part of the Journal of Geotechnical and Geoenvironmental Engineering, © ASCE, ISSN 1090-0241.

Table 1. Index, Mineralogy, and Cation Exchange Properties of Sodium Bentonite (Na-B) Sampled from the Test GCL

Measurement	Properties	Na-B GCL	Determination method
Index properties	Swell index (mL=2 g)	29.5	ASTM D5890-11 (ASTM 2011)
	Mass per unit area (kg=m^2)[a]	5.1	—
	Water content (%)	4.7	ASTM D2216-10 (ASTM 2010a)
	Loss on ignition (%)	2.06	Scalia (2012)
	Liquid limit (%)	481	ASTM D4318-10e1 (ASTM 2010b)
	Plastic limit (%)	451	
Mineralogy	Montmorillonite (%)	84	X-ray diffraction
	Quartz (%)	9	
	Plagioclase(%)	3	
	Clinoptilolite (%)	2	
	Illite, mica, orthoclase (%)	1	
	Average calcite by mass (%)	1.03	ASTM D4373-14 (ASTM 2014)
Bound cations	$Na^{þ}$	30.5	ASTM D7503-10 (ASTM 2010c)
(cmol þ=kg)	$Ca^{2þ}$	28.8	
	$Mg^{2þ}$	8.4	
	$K^{þ}$	2.2	
	CEC (cmol^{þ}=kg)	81.0	

[a]Mass per unit area of the GCL was 5.7 kg=m^2.

Materials and Methods

GCL Specimens

The GCL used in this study contained granular Na-B encapsulated between a woven and nonwoven geotextile bound together by needle-punched fiber bundles. Mass per unit area of the nonwoven geotextile was 0.34 kg=m^2, and the mass per unit area of the woven geotextile was 0.15 kg=m^2. Table 1 summarizes results from index, mineralogy, and cation exchange tests conducted to characterize the properties of GCL and internal bentonite. GCL dry mass per unit area was 5.7 kg=m^2 and that of the bentonite was 5.2 kg=m^2. Average initial moisture content of the bentonite was 4.7%. Fig. 1 is a plot of bentonite granule size distribution (GSD) measured using mechanical sieve analysis. Median granule size (d_{50}) is ~1.0 mm. GSDs for a similar series of Na-B GCLs reported by Shackelford et al. (2000) are included on Fig. 1 for comparison and show similar GSD. Cation exchange capacity (CEC) and concentrations of bound cations ($Ca^{2þ}$, $Na^{þ}$, $Mg^{2þ}$ and $K^{þ}$) were determined by ASTM D7503-10 (ASTM 2010c). Average CEC was 81.0 cmol^{þ}=kg with $Na^{þ}$ being the predominant bound cation (30.5 cmol^{þ}=kg). The liquid limit (w_L) was 481% and plasticity index (PI) was 451%. X-ray diffraction (XRD) analyses indicated bentonite mineralogy of 84% montmorillonite, 9% quartz, 3% plagioclase, and ≤2% of clinoptilolite, illite, mica, orthoclase, and calcite. These index and compositional characteristics are consistent with values for Na-B GCLs reported in many previous studies.

A water vapor sorption isotherm was obtained for a ~3-g sample of the bentonite along a wetting and subsequent drying path using a dynamic dew point sorption analyzer at a temperature of 25°C (VSA Apparatus, Decagon Devices, Pullman, Washington) (Likos et al. 2011). A water vapor sorption isotherm is a characteristic property of a material that describes the relationship between relative humidity (RH) and the equilibrium moisture content (w) of that material at a specified temperature. The GCL bentonite isotherm (Fig. 2) displays hysteresis and wavy behavior commonly attributed to successive adsorption or desorption of zero, one, and two molecular water layers in the expandable interlayer of the montmorillonite mineral fraction (e.g., Likos and Lu 2006; Likos and Wayllace 2010).

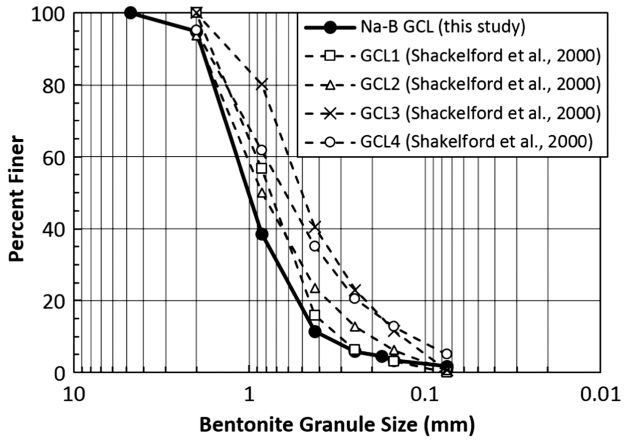

Fig. 1. Granule size distribution of air-dry sodium bentonite (Na-B) sampled from the test GCL

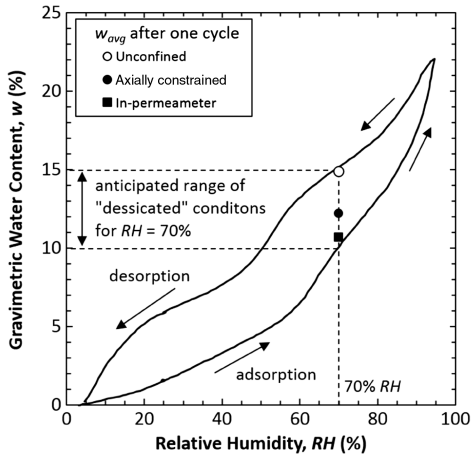

Fig. 2. Water vapor sorption isotherm for sodium bentonite (Na-B) sampled from the test GCL

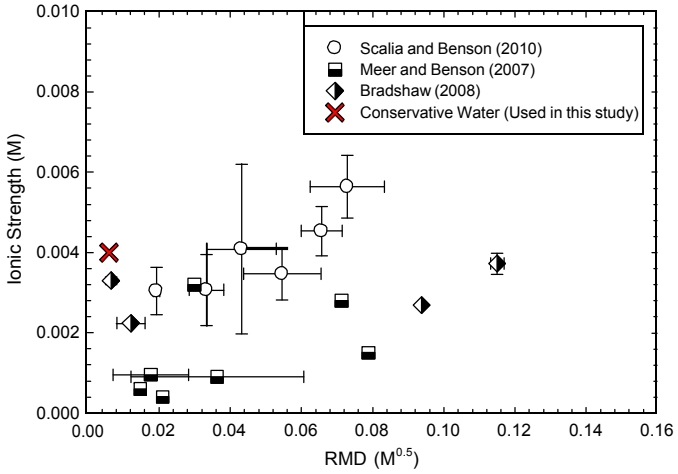

Fig. 3. Ionic strength versus RMD of pore water eluent solutions from representative landfill cover and subgrade soils (data from Scalia and Benson 2010)

For the purposes of this study, the measured sorption isotherm was used to quantify and subsequently verify bentonite water content corresponding to an unambiguously defined air-dry condition. In a similar study, for example, Lin and Benson (2000) cyclically permeated and desiccated Na-B GCL specimens by exposing them to ambient laboratory conditions until specimen mass ceased to change. RH during the drying phase was estimated to be approximately 50% during the drying phase but was not directly controlled and was likely to vary during the drying process. A specific RH value of 70% was selected in the current study to explicitly define air-dry conditions and to afford control over the drying environment, thereby allowing three different desiccation approaches to be systematically compared. According to the bentonite's sorption isotherm (Fig. 2), 70% RH corresponds to gravimetric water content ranging from approximately 10 to 15% depending on wetting direction (e.g., w ~ 10% along the wetting path and w ~ 15% along the drying path). As subsequently described in more detail, the three individual data points on Fig. 2 are equilibrium bentonite water content values measured after a desiccation cycle under controlled 70% RH conditions following each of three drying approaches.

Permeant Solutions

Permeant solutions were prepared using deionized water (DW) as a control and conservative-water (CW) representing a lower bound of pore fluid chemistries for typical landfill cover soils. Scalia and Benson (2010) collected cover soils from various landfills around the United States, performed column elution tests to collect and analyze the pore water, and compiled these data along with results from similar studies (Meer and Benson 2007; Bradshaw 2008). Fig. 3 summarizes those pore fluid chemistries in the space of ionic strength (I) and the relative abundance of monovalent and divalent cations (RMD), where Kolstad et al. (2004) defined RMD as:

$$RMD = \frac{M_M}{\sqrt{M_D}} \quad (1)$$

where M_M = total molar concentration of monovalent cations; and M_D = total molar concentration of divalent cations. CW has RMD near the lower bound of the observed field data (i.e., predominantly divalent cations) and average ionic strength and is thus intended to yield a potentially conservative (i.e., relatively high) measurement of hydraulic conductivity in cases where the chemical characteristics of permeant water in the field are unknown (Scalia and Benson 2010). CW for this study was synthesized by dissolving reagent-grade NaCl and $CaCl_2$ salts in DW. Solution characteristics are summarized on Table 2.

Hydration and Permeation Procedures

GCL specimens were permeated in flexible-wall permeameters for hydraulic conductivity measurements according to ASTM D5084 (ASTM 2003), Method B (falling headwater-constant tail water). An additional nonwoven geotextile was placed on both sides of the GCL during permeation and desiccation. Geotextiles were used in lieu of porous stones and filter paper because the geotextiles had a lower air-entry pressure. This facilitated displacement of water from the top and bottom specimen boundaries using the regulated gas flow during in-permeameter testing. The GCL was not removed from the permeameter, and so, the boundary geotextiles remained in contact with the GCL during all times. After desiccation, the permeameter was resaturated with hydrating liquid. A graduated glass pipette with 5.4-mm inside diameter was used as the headwater reservoir and to measure influent flux for calculating k. Specimens were prepared by cutting a circular specimen (diameter = 104 mm) from the GCL roll using a razor blade and a steel ring following methods outlined in Jo et al. (2001). The geotextile fibers of the GCL were trimmed using a small scissors to prevent formation of preferential flow paths along the edge. Bentonite around the specimen perimeter was hydrated with permeant solution during cutting to prevent loss due to exposure at the specimen edge. Specimen thickness was measured with calipers at six equidistant points around the perimeter. This ranged from 6.1 to 10.5 mm and averaged 8.3 mm. The GCL was then overlain and underlain by a geotextiles, placed in the permeameter, encased in a latex membrane, and isotropic effective confining pressure of 20 kPa was applied to simulate approximately one meter of soil in a final cover system. The influent valve of the permeameter was initially opened to hydrate the GCL for 48 h while keeping the effluent valve closed. After 48 h, both lines were flushed to remove air bubbles and then bottom-to-top flow through the specimen was initiated. An average hydraulic gradient of 30 was maintained during the permeation phase. Permeation was continued until each of the following termination criteria were met per ASTM D5084 (ASTM 2003): (1) no systematic trend was observed in k over time; (2) at least four consecutive k readings were within ±25% of the mean; (3) at least four consecutive observations of effluent-to-influent flow ratio were within 1.0 ± 0.25.

Desiccation Procedures

The unconfined desiccation approach was designed to be similar to that used in several previous cyclic wet-dry experiments (Shan and Daniel 1991; Daniel et al. 1993; Lin and Benson 2000). At the completion of each hydration/permeation phase, the confining cell

Table 2. Chemistry of Permeant Solutions Used for Hydraulic Conductivity Testing

Permeant solution	Abbreviation	NaCl (M)	$CaCl_2$ (M)	I (M)	RMD ($M^{0.5}$)	pH	Electrical conductivity (μS=cm)
Deionized water	DW	<0.005	<0.005	$<1.3 \times 10^{-7}$	undf	6.5	18.9
Conservative water	CW	0.0003	0.0019	0.004	0.006	6.0	442

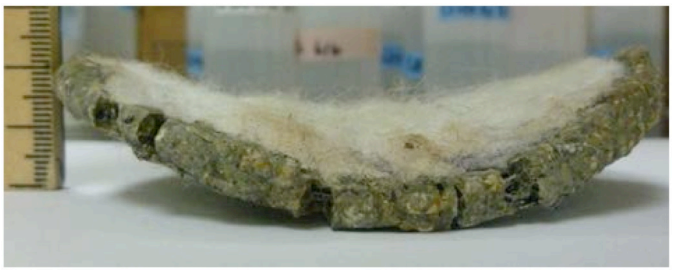

Fig. 4. Photo of curling deformation observed during desiccation for unconfined GCL specimens

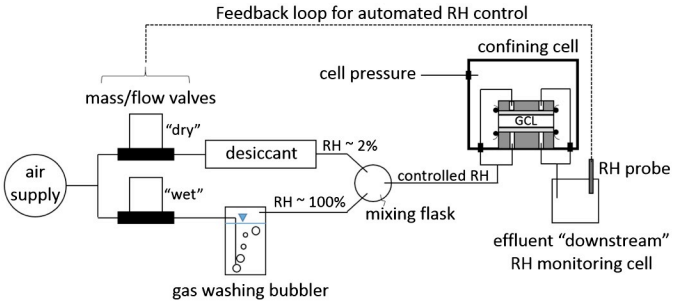

Fig. 5. Schematic of end-cap flushing system for the in-permeameter test method

pressure was released so that the permeameter could be drained and disassembled. The GCL was removed from the base pedestal and carefully separated from the end caps and latex membrane by hand (the geotextiles were not removed). Specimens were then moved into a small environmental chamber and placed directly on a flat, unlubricated surface with no external stress applied. Humidity was maintained at 70% RH using a household humidifier system (Honeywell HCM-6009, Palatine, Illinois) and continuously monitored with a capacitance-film humidity/temperature probe having a range of 0 to 99% RH and 0.01% RH resolution (Model HMI-35, Vaisala Corporation, Boulder, Colorado). If measured RH deviated from the 70% target by ±5%, the controls on the humidifier were manually adjusted. RH could be maintained using this approach to 73.7% ± 4.3% during a typical cycle. Corresponding temperature averaged 19.6 ± 2.0°C. Specimens were periodically weighed to monitor the drying-induced weight loss until mass ceased to change. As illustrated in Fig. 4, several of the specimens underwent extensive curling deformations, and the cross section became distorted from a circular shape. Bentonite paste (Na-B and permeant water mixture) was applied along the edges of such specimens to prevent preferential flow along during rehydration and permeation.

The axially constrained desiccation approach incorporated two perforated PVC disks above and below the GCL. The purpose of these disks was to provide rigidity to the specimen and thus limit disturbance from handling, while still allowing evaporation through the perforations (drilled holes having ~6 mm diameter and evenly spaced ~15 mm on center). Specimens were desiccated in the same controlled RH environment as the unconfined specimens (RH ¼ 70%), but under an applied vertical stress (dead load) of 20 kPa. Specimens in these tests were removed from the base pedestal, but the top and bottom end caps, latex membrane, and O-ring seal between the membrane and endcaps were left intact, such that evaporative drying could occur axially through the perforated end caps. Specimens were periodically weighed, and desiccation was considered complete when specimen mass ceased changing. Although this approach was intended to minimize disturbance resulting from extensive specimen handling and drying-induced curling, it should be noted that it does require removing the GCL from the confining cell after each hydration/permeation phase, thus causing a temporary and potentially nonrepresentative change in total stress.

The in-permeameter desiccation approach involved integration of a controlled-humidity air stream directly into the specimen end caps to actively dry the specimen without disassembly or removal from the permeameter. This prevented disruption of applied total stress and eliminated potentially disturbing specimen handling. This basic approach has been adopted in a variety of forms for measuring mechanical properties of unsaturated soils (e.g., stress/strain and strength) and has typically involved circulation of dry or humid gas (usually air) through the specimen end cap(s) in triaxial or oedometer systems (e.g., Blatz et al. 2008). Humidity control in such systems has commonly been achieved using salt or acid solutions and is practical for controlling RH between approximately 10 and 90%. This corresponds to total suction between approximately 300 and 15 MPa at 20°C. Although active circulation of gas in such systems has been shown to accelerate soil drying processes, equilibration times can still be quite long depending on diffusion path length (i.e., specimen geometry and boundary conditions) and have been measured on the order of approximately 50 days or more for typical triaxial specimens (e.g., Blatz et al. 2008). The thin geometry of GCL specimens, on the other hand, makes the approach particularly amenable to a relatively short equilibration time.

The automated humidity control approach described by Likos and Lu (2003) was adapted to circulate a controlled-humidity air stream through the top and bottom specimen caps. As illustrated on Fig. 5, laboratory air was routed into two separate gas streams through a pair of computer-controlled mass/flow valves (MKS Instruments, Type 1179A). The first air stream was bubbled through a gas-washing bottle filled with DW, resulting in a nearly vapor-saturated or wet air stream at RH approaching 100%. The second gas stream was routed through a column containing $CaSO_4$ desiccant, which resulted in a desiccated or dry air stream with RH of approximately 2%. The wet and dry streams were then mixed at a combined flow rate of either 200 or 500 cm^3=min, resulting in a humid gas stream having RH that depended on the wet-to-dry gas flow ratio. For the tests reported here, the humid gas stream was set to automatically target 70% RH and was routed through the top and bottom end caps on either side of the GCL specimen until equilibrium was achieved. A capacitance humidity probe (Vaisala Corporation, Model HMI-35) was used to measure effluent RH in a monitoring cell located on the downstream side of the GCL and thus formed a feedback loop with a control computer for automated regulation of the wet-to-dry gas flow ratio. Equilibrium was considered complete when measured RH on the downstream side of the GCL reached 70% and maintained that value for three to five days. For the permeation phase of testing, the air-flow system was disconnected from the permeameter by closing valves on the confining cell and replacing the connections with the falling head-water pipette and constant tail-water reservoir (not shown on Fig. 5) for permeation and k determination according to ASTM D5084 (ASTM 2003).

Image and Water Content Analysis

Three sacrificial GCL specimens were prepared for destructive analysis after one permeation/desiccation cycle. These specimens were hydrated and permeated using DW as the permeant solution and desiccated following each of the three approaches. A sharp scalpel was used to cut the needle stitching fibers so that the woven

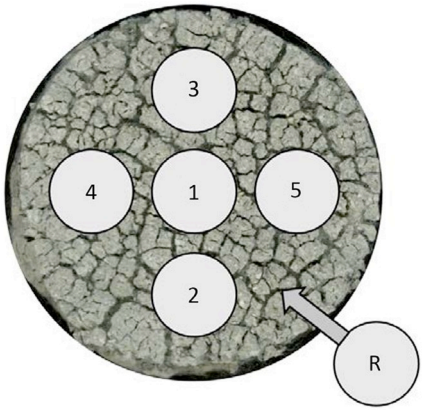

Fig. 6. Approximate sampling locations for postdesiccation measurement of gravimetric water content; samples included material from six discrete locations and the remainder (R) of the specimen

geotextile could carefully be peeled away from the bentonite layer. Images of desiccation crack patterns were obtained by placing the exposed bentonite layer directly on the scanning window of a 1,200 dots per inch (dpi) color image scanner (Epson B11B198011, Long Beach, California). Bentonite samples were then taken from five distributed locations on the GCL and from the remaining (R) material (Fig. 6) to determine and compare the spatial uniformity of gravimetric water content obtained using each desiccation approach.

Raw images from the scanner were 10,281 by 13,305 pixels and 215.9 by 279.4 mm in size, which resulted in a pixel size of 0.021 mm. A square image of 2,400 by 2,400 pixels was cropped from the center of the raw image for processing. Processing steps included conversion to 8-bit greyscale, morphological closing, and greyscale thresholding to obtain a binary (black and white) image used to differentiate regions of bentonite (white) from regions of cracks (black). Additional processing refinements included morphological opening, removal of white areas smaller than 1,000 square pixels within black regions, and removal of black pixel areas smaller than 1,000 square pixels within white regions. Although nondestructive (X-ray) imaging approaches for desiccation crack analysis of GCLs have been demonstrated, there are challenges with phase contrast and resolution for thin clay specimens (e.g., Potvin et al. 2011). A destructive approach was adopted in this study to maximize image resolution, to improve greyscale contrast, and to accommodate direct water content sampling as described previously.

Cracking patterns observed in the desiccated bentonite demonstrated features consistent with previous desiccation studies of GCLs and other clay and nonclay materials (e.g., Groisman and Kaplan 1994; Miller et al. 1998; Lin and Benson 2000; Tang et al. 2008; Azad et al. 2011; Costa et al. 2013). Notable features include isolated bentonite segments, herein called cells, separated by a network of orthogonal or nonorthogonal cracks of various thicknesses. Quantitative parameters calculated from the processed images included crack intensity factor (CIF), the total number of bentonite cells (N_{cell}), average bentonite cell area ($A_{cell;avg}$), maximum bentonite cell area ($A_{cell;max}$), average crack width ($W_{cr;avg}$), maximum crack width ($W_{cr;max}$), and frequency histograms of cell area and crack width. CIF was defined as proposed by Miller et al. (1998) in the context of desiccation cracking of compacted clay liner materials:

$$\text{CIF}\ (\%) = \frac{\sum A_{cr}}{A_t} \qquad (2)$$

where ΣA_{cr} = total projected area of cracks; and A_t = total projected area of the image. Crack width and orientation were quantified by intensity gradient analysis, where the direction of smallest intensity change gives orientation of cracks and the direction of largest intensity change gives edges of cracks (Maini and Aggarwal 2009). Crack width was determined by distance transform within the identified crack regions (Huang and Mitchell 1994).

A preliminary series of verification analyses was conducted using black and white images containing simulated bentonite cells of known area (triangular, circular, rectangular, and square shapes ranging in size from 10 to 20 mm^2). These tests indicated that the simulated cell areas could be measured with an error of less than 1%. Similar analyses of images containing simulated cracks (intersecting black lines of known thickness ranging from 0.1 to 2.2 mm) indicated that line thickness could be measured with an error of less than 2% for line thicknesses greater than 1.0 mm. Resolving thinner lines resulted in progressively more error, but this remained less than 5% for line thickness as small as 0.4 mm and less than 18% for line thickness as small as 0.1 mm.

Results and Discussion

Cycle Duration

Table 3 is a summary of cycle duration, water content uniformity, and quantitative image analysis parameters measured for each of the three test methods. Reported cycle durations are the average amount of time required to reach steady state for permeation and desiccation cycles. Required permeation times, which range from 17 to 30 days, are far more comparable among the methods than the required desiccation times, which range from 14 to 108 days. By far the longest desiccation time (108 days) was required for the axially constrained method. This observation is interpreted to reflect inhibited evaporation through the rigid PVC plates used to provide structural support to the GCL during disassembly and removal from the permeameter.

The in-permeameter method required the least amount of time for desiccation. This is interpreted to reflect active flow of dry air through both the top and bottom end caps and adjacent geotextile layers. Desiccation time was also found to depend on flow rate of the dry gas stream. This is illustrated in Fig. 7, which shows a time series of RH measured on the downstream side of the GCL at two different total air flow rates: 200 and 500 cm^3=min. Downstream

Table 3. Cycle Duration, Uniformity, and Quantitative Image Analysis Parameters for Three Desiccation Test Procedures

	Cycle duration[a]		Drying uniformity		Image analysis parameters					
Desiccation method	Wet (d)	Dry (d)	w_{avg} (%)	COV (%)	CIF	N_{cell}	$A_{cell;avg}$ (mm^2)	$A_{cell;max}$ (mm^2)	$W_{cr;avg}$ (mm)	$W_{cr;max}$ (mm)
Unconfined	17	14	14.9	3.9	31.8	182	9.5	57.4	0.52	2.11
Axially constrained	30	108	12.2	2.4	32.7	166	10.5	43.3	0.59	2.24
In-permeameter	20	11[b]	10.7	2.8	32.8	190	9.1	41.8	0.50	1.78

[a]Average cycle duration using both DW and CW permeant solutions.
[b]Gas flow rate of 500 cm^3=min.

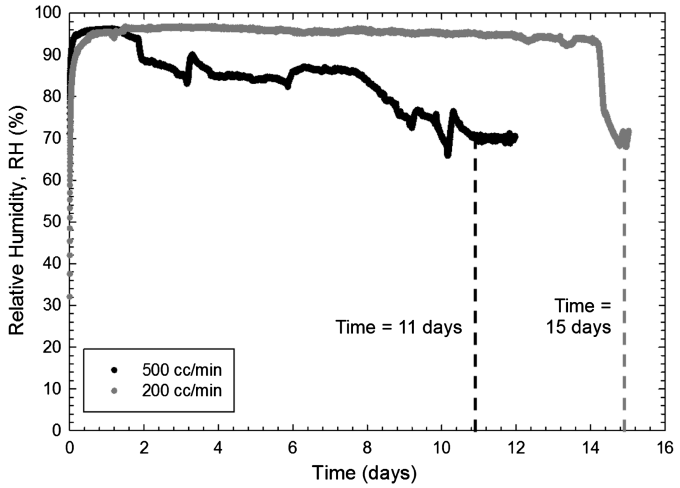

Fig. 7. Relative humidity (RH) measured downstream of the GCL specimen at two gas flow rates

RH in both cases is initially near the upper limit of the measurement probe (~98%), indicating substantial transfer of water vapor from the GCL into the gas stream (i.e., evaporative drying of the GCL). For a gas flow rate of 200 cm^3=min, high downstream RH is maintained fairly steadily for approximately 14 days and then drops to the target value of 70% RH over a relatively short span of approximately one day. For the faster gas flow rate of 500 cm^3=min, the downstream RH approaches the 70% target more gradually and reaches steady state in approximately 11 days.

Water Content Uniformity

Water content information on Table 3 includes average gravimetric water content (w_{avg}) and corresponding coefficient of variation (COV) from the spatially distributed samples (Fig. 6) taken after one desiccation cycle. Average water content in the desiccated condition is 14.9, 12.2, and 10.7% for the unconfined, axially constrained, and in-permeameter methods, respectively. Disparity in these results suggests some variation in the extent of drying achieved among the three methods, despite the fact that all three involved drying under similarly controlled RH conditions. All three values are within the bounds defined by the wetting and drying loops of the water vapor sorption isotherm (Fig. 2), confirming that equilibrium was likely achieved in each case. The fact that water content obtained using the unconfined test procedure falls close to the desorption bound suggests that the drying process may replicate an initial drying path. Conversely, the fact that water content obtained using the in-permeameter method falls close to the adsorption bound suggests that this method may replicate an initial wetting process.

Coefficients of variation (COV) summarized on Table 3 are calculated as the standard deviation in spatially distributed water content divided by the mean. COV for the three methods ranges from 2.4 to 3.9%. These small and similar COV values indicate that all three methods result in very uniform drying across the surface of the GCL. The smallest COV for the axially constrained method (COV ¼ 2.4%) may also be a reflection of its relatively long dry cycle duration (108 days), which may result in a more uniform water content distribution.

Quantitative Image Analysis

Fig. 8 is a series of raw (unprocessed) images of the bentonite surface after one desiccation cycle following the unconfined [Fig. 8(a)], axially constrained [Fig. 8(b)], and in-permeameter [Fig. 8(c)] test methods. Table 3 summarizes corresponding image analysis parameters, including CIF, total number of bentonite cells (N_{cell}), average and maximum bentonite cell size ($A_{cell;avg}$, $A_{cell;max}$), and average and maximum desiccation crack width ($W_{cr;avg}$, $W_{cr;max}$). CIF for the unconfined, axially constrained, and in-permeameter desiccation methods is 31.8, 32.7, and 32.8%, respectively, indicating that total crack areas for all three methods are very similar. There is systematic correlation between CIF and average desiccated water content (w_{avg}), which does substantially vary among the three methods. For example, the lowest mean water content (10.7%) obtained using the in-permeameter method corresponds to the highest CIF (32.8%). The highest mean water content (14.9%) obtained using the unconfined method corresponds to the lowest CIF (31.8%). This

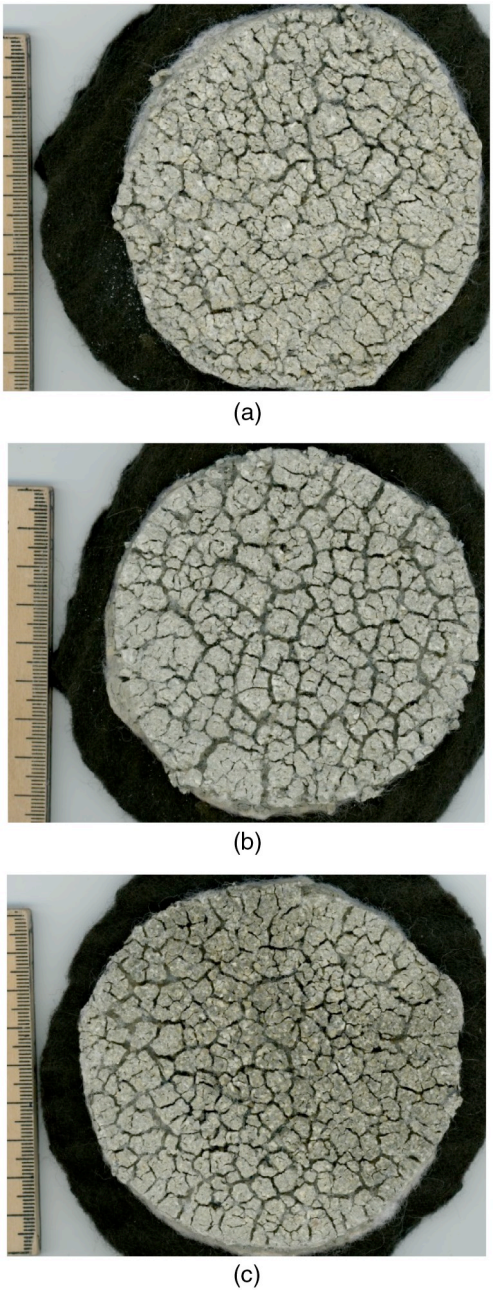

Fig. 8. Raw images of GCL desiccation crack patterns after one drying cycle: (a) unconfined method; (b) axially constrained method; (c) in-permeameter method

observation is consistent with the fact that cracking propagates as drying continues and suggests that the extent of cracking ultimately reaches some upper bound.

Average bentonite cell area for the unconfined, axially constrained, and in-permeameter methods were 9.5, 10.5, and 9.1 mm^2, respectively. Although these values appear similar, p-values obtained from a statistical t-test of the data set are less than 0.005, indicating that the cell area distributions are statistically different from each other. Average crack width for the unconfined, axially constrained, and in-permeameter methods were 0.52, 0.59, and 0.50 mm, respectively. Corresponding p-values were also less than 0.005. Maximum crack width ranges from 1.78 to 2.24 mm. This range is consistent with field observations of exhumed in-service GCLs, where desiccation cracks as wide as 2 mm have been measured (Melchior 2002).

As noted in Table 3, larger bentonite cell area systematically corresponds to larger crack widths. This observation is consistent with similar studies in the literature (e.g., Tang et al. 2008). The largest crack widths ($W_{cr;avg}$ ¼ 0.59 mm, $W_{cr;max}$ ¼ 2.24 mm) were obtained for the axially constrained method, which also resulted in the smallest number of bentonite cells (N_{cell} ¼ 166) and largest average cell area ($A_{cell;avg}$ ¼ 10.5 mm^2). Conversely, the in-permeameter method resulted in the smallest crack widths ($W_{cr;avg}$ ¼ 0.50 mm, $W_{cr;max}$ ¼ 1.78 mm), the largest number of bentonite cells (N_{cell} ¼ 190), and the smallest average cell area ($A_{cell;avg}$ ¼ 9.1 mm^2).

Controlling Factors for Crack Initiation in Constrained GCLs

Controlling factors in desiccation cracking of clays and other materials include tensile stress and strain energy that develop when the material is restrained against shrinkage (Costa et al. 2013). Shrinkage can be constrained in several ways, including frictional or other traction or displacement boundary conditions, stress concentrations resulting from internal flaws or nonuniform drying, and intrinsic heterogeneities in soil texture and structure (e.g., Peron et al. 2009). In many previous studies of clay systems undergoing free shrinkage, (e.g., drying of clay patties in shallow circular dishes), tensile stress distribution is controlled largely by material stiffness and basal adhesion at the lower boundary (i.e., friction at the interface between the clay and the dish that contains it) (e.g., Costa et al. 2013). Basal boundary conditions with more friction (e.g., thick clay specimens) tend to produce fewer, wider cracks with larger cell areas, whereas boundary conditions with less friction (e.g., thin clay specimens) tend to produce thinner cracks with smaller cell areas.

Differences observed here highlight important differences between free shrinkage of clay patties in shallow dishes and constrained shrinkage of GCLs as imposed by the geotextile layers and confining conditions. Although there appear to be some systematic trends in the image analysis parameters noted previously, it is clear that the intensity and pattern of cracking among the three different desiccation approaches are very similar. There is simply not much difference between CIF, $A_{cell;avg}$, and $W_{cr;avg}$ among the three methods. This similarity suggests that the mechanisms of crack initiation and propagation among the three methods are also similar, despite the fact that the stress boundary conditions during drying and extent of specimen handling are very different. All other things being equal, the unconfined desiccation method likely offers the least amount of shrinkage restraint and thus might be expected to result in thinner cracks and smaller cell areas. The axially constrained and in-permeameter methods, where shrinkage proceeds under applied external stress, likely offers more shrinkage restraint and thus might be expected to result in thicker cracks and larger cell areas. Lack of conclusive evidence for these expectations suggests that the boundary and internal stress distribution in a GCL are not as straightforward as the case for a clay patty shrinking in a shallow dish.

Shrinkage strains in GCLs may be affected by the properties of the geotextiles, variations in anchorage provided by needle punching fibers, and the uniformity of bentonite distribution within the sample (Bostwick et al. 2010; Rowe et al. 2011; Potvin et al. 2011). Needle-stitching the geotextiles and bentonite together not only creates more complex boundary conditions for shrinkage restraint (e.g., as evidenced by the curling deformations in Fig. 4), but the fiber bundles within the bentonite may also act as internal flaws that become controlling factors for crack initiation (Costa et al. 2013). Qualitative observation of crack intersection geometry for all three desiccation methods indicates a mixture of both orthogonal and nonorthogonal cracks. The orthogonal cracks are likely associated with crack propagation from sequential subdivision of bentonite cells during slow drying, whereas the nonorthogonal cracks may be associated with simultaneous cracking initiated at sites occupied by fiber bundles. Cracks observed in samples desiccated using all three methods did in fact appear to originate from fiber bundles, but the presence of fibers did not guarantee crack initiation at each location. It was difficult to quantify the fiber bundle size and frequency because the bundles were scattered throughout the desiccated GCL (i.e., they were not concentrated only in the crack junctions). Although a high prevalence of cracks originated from the fiber bundles, smaller fiber bundles appeared within the bentonite nodules as well. Nonetheless, the fact that bentonite cell size and crack width appear independent of external load and confining conditions suggests that internal flaws imposed by the fibers, rather than shrinkage restraint imposed by the stress boundary conditions, control crack initiation and propagation in GCLs. From a practical testing perspective, this implies that results of cyclic wet-dry experiments for GCLs obtained using relatively simple methods, such as unconfined desiccation, might be considered comparable to results obtained using more complex stress-controlled methods, such as the in-permeameter method.

Hydraulic Conductivity

Fig. 9 is a plot of steady-state hydraulic conductivity (k) measured after initial hydration and each subsequent wet-dry cycle. Fig. 9(a) includes results obtained for each of the three desiccation methods using DW as the permeant solution. Fig. 9(b) includes results obtained using CW. It should be noted that tests using the unconfined method and DW [solid circles in Fig. 9(a)] were terminated after the first testing cycle because of equipment constraints in the laboratory. In lieu of these measurements, therefore, results obtained by Lin and Benson (2000) for a similar Na-B GCL specimen using DW and similar unconfined desiccation procedures are reported for comparison with the other methods examined here.

Initial k after hydration using either DW or CW falls within a narrow band ranging from a minimum of approximately 2×10^{-11} m=s to a maximum of approximately 7×10^{-11} m=s. Initial k values using CW as the permeant solution are slightly higher (1.2 to 1.6 times) than initial k values obtained using the same apparatus with DW as the permeant solution. These observations are consistent with typically measured k values for Na-B GCLs using DW and dilute salt solutions under stresses characteristic of final covers (e.g., Shan and Daniel 1991; Lin and Benson 2000; Jo et al. 2001; Scalia and Benson 2011).

Hydraulic conductivity using DW [Fig. 9(a)] remains essentially unaffected for as many as three, five, or seven wet-dry cycles using

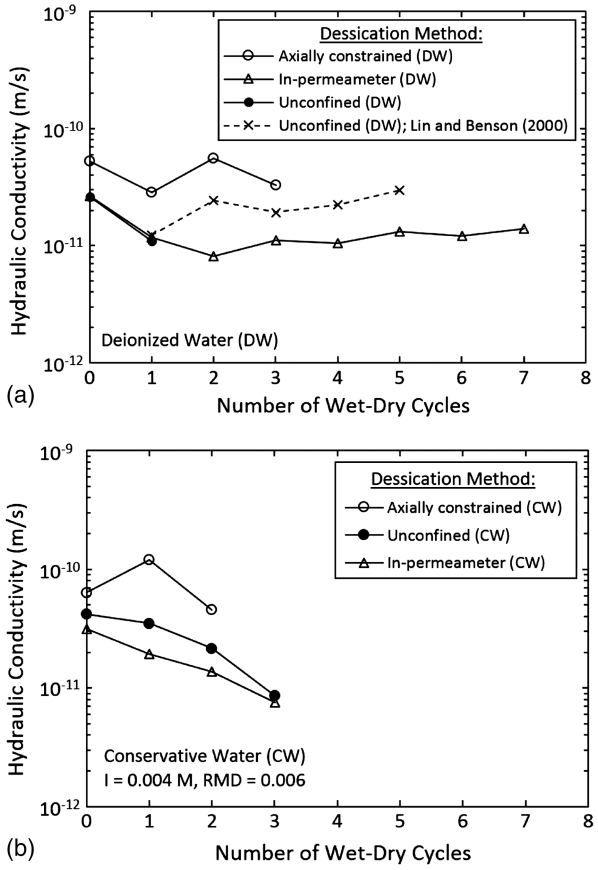

Fig. 9. Hydraulic conductivity with wet-dry cycles using (a) deionized water (DW); (b) conservative water (CW) permeant solutions

the axially constrained, unconfined, and in-permeameter methods, respectively. The change in k from any one measurement to any subsequent measurement is not greater than a factor of two for the axially constrained and unconfined methods and not greater than a factor of 1.5 for the in-permeameter method (after an initial decrease by a factor of 3.25 over the first two cycles). Hydraulic conductivity using CW also remains essentially unaffected over two measured cycles using the axially constrained approach but drops slightly (by a factor of 4 to 5) from initial hydration to the third cycle using the unconfined and in-permeameter test approaches. A similar decrease in k by a factor of 6 was observed during the first three wet-dry cycles in Lin and Benson's (2000) experiments using 0.0125-M $CaCl_2$.

Shan and Daniel (1991) conducted hydraulic conductivity tests on a Na-B GCL using tap water as a permeant liquid and reported results showing that k was essentially unaffected ($\sim 1.8 \times 10^{-11}$ m=s) after four wet-dry cycles. Lin and Benson's (2000) experiments demonstrated that wet-dry cycling using DW and tap water had little effect on hydraulic conductivity of Na-B GCLs after four wet-dry cycles ($\sim 1 \times 10^{-11}$ m=s) but increased to as much as 7.6×10^{-8} m=s using 0.0125 M $CaCl_2$ solution, an observation attributed to cation exchange and desiccation cracks that did not fully heal upon rehydration. A similar increase cannot be observed in the current study given the limited number of cycles, but it is clear that k is not significantly affected by the desiccation method over the numbers of cycles that are measured. The image analysis results indicate that the extent and pattern of cracking is similar among the three methods. Results from hydraulic conductivity testing indicate that this extent of cracking does not prevent full healing upon rehydration using either DW or CW as the permeant solution.

Summary and Conclusions

Experiments in this study have been designed to examine three alternative laboratory methods for cyclic wet-dry testing of geosynthetic clay liners. Na-B GCL specimens were initially permeated and then subjected to one of three desiccation techniques: (1) unconfined desiccation, whereby specimens were removed from the permeameter and dried under zero external load, (2) axially constrained desiccation, whereby specimens were removed from the permeameter and dried between two rigid platens under axial stress, and (3) in-permeameter desiccation, whereby specimens were desiccated by circulating humidity-controlled air through the top and bottom end caps. Quantitative image analysis was used to compare desiccation crack patterns after one wet-dry cycle for a set of sacrificial GCL specimens.

The average amount of time required for the permeation phase is comparable among the three methods and ranges from 17 to 30 days. Average desiccation times for the unconfined and in-permeameter methods are comparable (14 and 11 days, respectively) but are significantly longer for the axially constrained method (108 days). All three methods produce a highly uniform spatial distribution of bentonite water content in the desiccated state. Image analysis indicates similarity in desiccation crack intensity and pattern among the three testing approaches, despite the fact that stress boundary conditions during drying are very different. Because the cracking characteristics among the three methods are very similar, measured hydraulic conductivity values after cycles of permeation-desiccation are also similar. Initially low ($\sim 1 \times 10^{-11}$ m=s) hydraulic conductivity remains essentially unaffected for up to as many as seven cycles using deionized water (DW) as the permeant solution and up to as many as three cycles using conservative water (CW) characteristic of typical landfill cover soils. These observations highlight important differences between free shrinkage of clay patties in shallow dishes, as often reported in the literature, and constrained shrinkage of GCLs as imposed by the geotextile layers and confining conditions. Similarities in the cracking behavior and hydraulic response among the three methods are interpreted to indicate that internal flaws in the bentonite (e.g., reinforcing fiber bundles), rather than external stress conditions, may control crack initiation and propagation. From a practical testing perspective, the axially constrained method for cyclic wet-dry testing of GCLs appears to be an acceptable compromise between sample disturbance (unloading-reloading) and ease of execution, although it is relatively time-consuming.

References

ASTM. (2003). "Standard test method for measurement of hydraulic conductivity of saturated porous materials using a flexible wall permeameter." ASTM D5084, West Conshohocken, PA.

ASTM. (2010a). "Standard test methods for laboratory determination of water (moisture) content of soil and rock by mass." ASTM D2216-10, West Conshohocken, PA.

ASTM. (2010b). "Standard test methods for liquid limit, plastic limit, and plasticity index of soils." ASTM D4318-10e1, West Conshohocken, PA.

ASTM. (2010c). "Standard test method for measuring the exchange complex and cation exchange capacity of inorganic fine-grained soils." ASTM D7503-10, West Conshohocken, PA.

ASTM. (2011). "Standard test method for swell index of clay mineral component of geosynthetic clay liners." ASTM D5890-11, West Conshohocken, PA.

ASTM. (2014). "Standard test method for rapid determination of carbonate content of soils." ASTM D4373-14, West Conshohocken, PA.

Azad, F. M., Rowe, R. K., El-Zein, A., and Airey, D. W. (2011). "Laboratory investigation of thermally induced desiccation of GCLs in double composite liner systems." Geotext. Geomembr., 29(6), 534–543.

Benson, C., and Meer, S. (2009). "Relative abundance of monovalent and divalent cations and the impact of desiccation on geosynthetic clay liners." J. Geotech. Geoenviron. Eng., 10.1061/(ASCE)1090-0241(2009)135:3(349), 349–358.

Benson, C., Thorstad, P., Jo, H., and Rock, S. (2007). "Hydraulic performance of geosynthetic clay liners in a landfill final cover." J. Geotech. Geoenviron. Eng., 10.1061/(ASCE)1090-0241(2007)133:7(814), 814–827.

Blatz, J. A., Cui, Y.-J., and Oldecop, L. (2008). "Vapour equilibrium and osmotic technique for suction control." Geotech. Geol. Eng., 26(6), 661–673.

Boardman, T., and Daniel, D. (1997). "Hydraulic conductivity of desiccated geosynthetic clay liners." J. Geotech. Geoenviron. Eng., 10.1061/(ASCE)0733-9410(1996)122:3(204), 204–208.

Bostwick, L., Rowe, R. K., Take, W. A., and Brachman, R. W. I. (2010). "Anisotropy and directional shrinkage of geosynthetic clay liners." Geosynthetics Int., 17(3), 157–170.

Bradshaw, S. (2008). "Effect of cation exchange during subgrade hydration and leachate permeation." M.S. thesis, Univ. of Wisconsin, Madison, WI.

Costa, S., Kodikara, J., and Shannon, B. (2013). "Salient factors controlling desiccation cracking of clay in laboratory experiments." Géotechnique, 63(1), 18–29.

Daniel, D., Shan, H., and Anderson, J. (1993). "Effects of partial wetting on the performance of the bentonite component of a geosynthetic clay liner." Geosynthetics, 93, 1483–1496.

Egloffstein, T. (2001). "Natural bentonites—Influence of the ion exchange and partial desiccation on permeability and self-healing capacity of bentonites used in GCLs." Geotext. Geomembr., 19(7), 427–444.

Groisman, A., and Kaplan, E. (1994). "An experimental study of cracking induced by desiccation." Europhys. Lett., 25(6), 415–420.

Henken-Mellies, W., Zanzinger, H., and Gartung, E. (2002). "Long-term field test of a geosynthetic barrier in a landfill cover system." Clay geosynthetic barriers, H. Zanzinger, R. Koerner, and E. Gartung, eds., 303–309.

Huang, C. T., and Mitchell, O. R. (1994). "A Euclidean distance transform using grayscale morphology decomposition." IEEE Trans. Pattern Anal. Mach. Intell., 16(4), 443–448.

James, A., Fullerton, D., and Drake, R. (1997). "Field performance of GCL under ion exchange conditions." J. Geotech. Geoenviron. Eng., 10.1061/(ASCE)1090-0241(1997)123:10(897), 897–901.

Jo, H., Benson, C. H., Shackelford, C. D., Lee, J., and Edil, T. B. (2005). "Long-term hydraulic conductivity of a non-prehydrated geosynthetic clay liner permeated with inorganic salt solutions." J. Geotech. Geoenviron. Eng., 10.1061/(ASCE)1090-0241(2005)131:4(405), 405–417.

Jo, H., Katsumi, T., Benson, C., and Edil, T. (2001). "Hydraulic conductivity and swelling of non-prehydrated GCLs permeated with single species salt solutions." J. Geotech. Geoenviron. Eng., 10.1061/(ASCE)1090-0241(2001)127:7(557), 557–567.

Kolstad, D., Benson, C. H., and Edil, T. B. (2004). "Hydraulic conductivity and swell of non-prehydrated GCLs permeated with multispecies inorganic solutions." J. Geotech. Geoenviron. Eng., 10.1061/(ASCE)1090-0241(2004)130:12(1236), 1236–1249.

Likos, W., and Lu, N. (2003). "Automated humidity system for measuring total suction characteristics of clay." Geotech. Test. J., 26(2), 1–12.

Likos, W. J., and Lu, N. (2006). "Pore scale analysis of bulk volume change from crystalline swelling in $Na^{þ}$- and $Ca^{2þ}$-smectite." Clays Clay Miner., 54(4), 515–528.

Likos, W. J., Lu, N., and Wenszel, W. (2011). "Performance of a dynamic dew point method for moisture isotherms of clays." Geotech. Test. J., 34(4), 373–382.

Likos, W. J., and Wayllace, A. (2010). "Porosity evolution of free and confined bentonites during interlayer hydration." Clays Clay Miner., 58(3), 399–414.

Lin, L., and Benson, C. H. (2000). "Effect of wet-dry cycling on swelling and hydraulic conductivity of GCLs." J. Geotech. Geoenviron. Eng., 10.1061/(ASCE)1090-0241(2000)126:1(40), 40–49.

Mackey, R., and Olsta, J. (2004). "Performance of geosynthetic clay liners used in two landfill closures in a coastal area of Florida." Advances in Geosynthetic Clay Liners Technology, R. Mackey and K. von Maugeuge, eds., ASTM, West Conshohocken, PA, 53–71.

Maini, R., and Aggarwal, H. (2009). "Study and comparison of various image edge detection techniques." Int. J. Image Proc., 3(1), 1–9.

Mazzieri, F. (2011). "Impact of desiccation and cation exchange on the hydraulic conductivity of factory-prehydrated GCLs." Proc., GeoFrontiers, ASCE, Reston, VA, 976–985.

Meer, S., and Benson, C. H. (2007). "Hydraulic conductivity of geosynthetic clay liners exhumed from landfill final covers." J. Geotech. Geoenviron. Eng., 10.1061/(ASCE)1090-0241(2007)133:5(550), 550–563.

Melchior, S. (2002). "Field studies and excavations of geosynthetic clay barriers in landfill covers." Proc., Int. Geosynthetic Clay Barriers Symp., H. Zanzinger, R. M. Koerner, and E. Gartung, eds., Swets and Zeitlinger, Lisse, Netherlands, 321–330.

Miller, C., Mi, H., and Yesiller, N. (1998). "Experimental analysis of desiccation crack propagation in clay layers." J. Am. Water Resour. Assoc., 34(3), 677–686.

Peron, H., Hueckel, T., Laloui, L., and Hu, L. B. (2009). "Fundamentals of desiccation cracking of fine-grained soils: Experimental characterization and mechanisms identification." Can. Geotech. J., 46(10), 1177–1201.

Potvin, J. J., Take, W. A., Siemens, G. A., and Kerr, A. (2011). "X Ray imaging of desiccation cracking patterns in geosynthetic clay liners." Proc., 14th Pan-Am Conf. on Soil Mechanics and Geotechnical Engineering and 64th Canadian Geotechnical Conf., Toronto.

Rowe, R. K., Bostwick, L. E., and Take, W. A. (2011). "Effect of GCL properties on shrinkage when subjected to wet-dry cycles." J. Geotech. Geoenviron. Eng., 10.1061/(ASCE)GT.1943-5606.0000522, 1019–1027.

Scalia, J. (2012). "Bentonite-polymer composites for containment applications." Ph.D. dissertation, Univ. of Wisconsin-Madison, Madison, WI, 247.

Scalia, J., and Benson, C. H. (2010). "Effect of permeant water on the hydraulic conductivity of exhumed GCLs." Geotech. Test. J., 33(3), 1–11.

Scalia, J., and Benson, C. H. (2011). "Hydraulic conductivity of geosynthetic clay liners exhumed from landfill final covers with composite barriers." J. Geotech. Geoenviron. Eng., 10.1061/(ASCE)GT.1943-5606.0000407, 1–13.

Shackelford, C. D., Benson, C. H., Katsumi, T., Edil, T. B., and Lin, L. (2000). "Evaluating the hydraulic conductivity of GCLs permeated with non-standard liquids." Geotext. Geomembr., 18(2-4), 133–161.

Shan, H., and Daniel, D. (1991). "Results of laboratory tests on a geotextile/bentonite liner material." Geosynthetics, 91, 517–535.

Sivakumar Babu, G. L., Sporer, H., Zanzinger, H., and Gartung, E. (2002). "Desiccation behavior of selected geosynthetic clay liners." Proc., Int. Symp. Clay Geosynthetic Barriers, Nuremberg, Germany, 295–302.

Sporer, H., and Gartung, E. (2002). "Laboratory tests on desiccation of geosynthetic clay liners." Proc., Int. Symp. Clay Geosynthetic Barriers, Nuremberg, Germany, 331–338.

Tang, C., Shi, B., Liu, C., Zhao, L., and Wang, B. (2008). "Influencing factor of geometrical structure of surface shrinkage cracks in clayey soils." Eng. Geol., 101(3-4), 204–217.